Iranian Journal of Science and Technology, Transactions of Civil Engineering (2022) 46:3485–3497
https://doi.org/10.1007/s40996-021-00789-3

RESEARCH PAPER

Hydraulic Analysis of Submerged Spillway Flows and Performance Evaluation of Chute Aerator Using CFD Modeling: A Case Study of Mangla Dam Spillway

Muhammad Kaleem Sarwar[1] · Zohaib Nisar[1] · Ghulam Nabi[1] · Faraz ul Haq[1] · Ijaz Ahmad[1] · Muhammad Masood[1] · Noor Muhammad Khan[1,2]

Received: 9 July 2021 / Accepted: 7 November 2021 / Published online: 20 November 2021

Abstract
Submerged spillways with large capacity outlets are generally provided below the dam crest to perform the dual functions of flood disposal and sediment flushing. Flood water passing through these spillways exhibits turbulent behavior. Moreover; hydraulic analysis of such turbulent flows is a challenging task. Therefore, the present study aims to use numerical simulations to examine the hydraulic behavior of submerged spillways constructed at Mangla Dam, Pakistan. Besides, the hydraulic performance of aerator was also evaluated at different operating conditions. Computational fluid dynamics code FLOW 3D was used to numerically model the flows of Mangla Spillway. Reynolds-averaged Navier–Stokes equations are used in FLOW 3D to numerically model the turbulent flows. The study results indicated that the developed model can simulate the submerged spillway flows as it computed the flow parameters with an acceptable error of up to 6%. Moreover, air concentration computed by model near spillway chute bed was 3% which raised to more than 6% after the installation of ramp on aerator which showed that developed model is also capable of evaluating the performance of submerged spillway aerator.

Keywords Aerator · CFD · FLOW 3D · Froude number · Submerged spillway

1 Introduction

Multi-purpose dams are used for water supply, irrigation, hydropower generation, and flood mitigation (Shao et al. 2020). Floods damages include economic damage and human lives; hence, vulnerable areas require mitigation measures to reduce flooding effects (Zhan et al. 2020). The spillway is a hydraulic structure that is provided in the dam body to safely pass the floods and reduces its damaging effects (Sarwar et al. 2020). Moreover, Pakistan, India, Nepal, and China are constructing multi-purpose reservoirs on their rivers. These rivers carry large sediments which are ultimately deposited in reservoirs (Chanel and Doering 2008; Jothiprakash et al. 2015).

The submerged spillway is a type of spillway used to release the flood water and flushing of reservoir sediments (Sarwar et al. 2016). Free surface flow and orifice-type flow occur in submerged spillways. Free surface flow takes place in case of low reservoir levels, while at high reservoir levels, spillway passes orifice-type flows (Bhosekar et al. 2012). Submerged spillways are built up with short length flat (profile slope $< 30°$) profile to facilitate the sediment flushing operation. These spillways hold the water head up to 90 m. Breast walls are supported by 6- to 8-m-thick piers. In submerged spillways, discharge intensities lie between 100 and 300 m^3/sec/m, leading to the flow depths of 10 to 12 m and Froude numbers between 3 and 6 (Bhosekar et al. 2012).

The operation of such spillways creates cavitational problems at spillway chutes due to high flow velocity (Lian et al. 2017). In order to avoid cavitational damages, chute aerators are provided. The aeration of spillway chute through aerators is considered the most economical and effective method (Sarwar et al. 2016).

✉ Muhammad Kaleem Sarwar
eng_kaleem@yahoo.com

[1] Centre of Excellence in Water Resources Engineering, University of Engineering and Technology, Lahore 54890, Pakistan

[2] Department of Civil Engineering, University of Engineering and Technology, Lahore 54890, Pakistan

Traditionally, hydraulic analysis of spillway flows and performance evaluation of aerators were carried out through physical model studies. However, scale modeling is time-consuming and expensive. Besides, it has scale effects and required skilled labor for its construction (Ho and Riddette 2010). Nowadays, numerical models are being used widely due to their ability to overcome the drawbacks of scale models. Computational fluid dynamics (CFD) is a numerical method used to model fluid flows. It solves the "Navier–Stokes" equations in three dimensions and can compute the fluid dynamics in a significantly improved manner. The application of CFD modeling for hydraulic analysis of spillway flows and performance evaluation of aerators is quite recent (Aydin 2018; Gadge et al. 2018, 2019; Gurav 2015; Jothiprakash et al. 2015; Teng et al. 2016; Teng and Yang 2016). Some other researchers like Bennett et al., (2018), Kumcu, (2017), and Yang et al., (2019) have also used CFD models to analyze the flows of different spillway projects. Another branch of CFD, i.e., particle methods in specific SPH (Shadloo et al. 2016; Ye et al. 2019; Luo et al. 2021), is also being applied for simulation of spillway flows (Saunders et al. 2014; Gu et al. 2017; Moreira et al. 2019, 2020). Thanks to its great performance in handling large deformation of phase boundaries/free surface, splashing, and flow fragmentations as demonstrated by O'Connor and Rogers (2021) and Shimizu et al. (2020), these studies indicate that CFD modeling has become a reliable design and analysis tool for spillway projects. However, very few studies are reported where submerged spillway flows were analyzed. In these studies, only submerged spillway with chute slope $> 10^0$ was focused.

In a spillway aerator study, Yang et al. (2020) performed 3D CFD modeling to understand the air–water flow behavior for a spillway of a large dam located in central Sweden and concluded that CFD models are very useful tools to quantify the air demand and air motion as physical models are unable to correctly model the airflow. Similarly, Aydin (2018) and Bhosekar et al. (2012) also conducted a numerical analysis of spillway aerators to judge their hydraulic performance which confirmed the ability of CFD models in two-phase flow (air and water) modeling. Results of these studies indicated that air concentration near bed of spillway was more (50%) for small gate opening and it decreased drastically 2 to 3% for low Froude numbers. Placing of deflector improved the air concentration in case of low Froude numbers. These studies evaluated the hydraulic performance of offset and deflector (ramp)-type aerators installed at submerged spillways. No study was found regarding performance evaluation of offset-cum-ramp-type aerators.

It is noted that hydraulic analysis of submerged spillway flows using CFD modeling specifically for very flat profile (chute slope $< 10^0$) submerged spillways is not reported much in the literature so far. Moreover, studies regarding performance evaluation of offset-cum-ramp-type aerators are also scanty; thus, there still remains gray area in the field of submerged spillway hydraulic and offset-cum-ramp-type aerators.

1.1 Mangla Dam Spillway

Mangla Dam, constructed in 1967 on Jhelum River, is the largest dam in Pakistan with a storage capacity of 8634 Mm^3. The main spillway of Mangla Dam is a submerged type provided with redial gates (Fig. 1). Spillway operates at a full gate opening of 10.7 m. The design discharge capacity of the spillway is 28600 m^3/s. Head above spillway crest is 52 m. The total length of the spillway is 135 m. It consists of three monoliths, which are separated by 7-m-wide piers. The spillway is provided with a flat slope parabolic chute and a two-stage stilling basin. Due to high flow velocities (up to 30 m/s), a chute aerator is constructed at the end of the horizontal floor of the Mangla Dam Spillway as shown in Fig. 1.

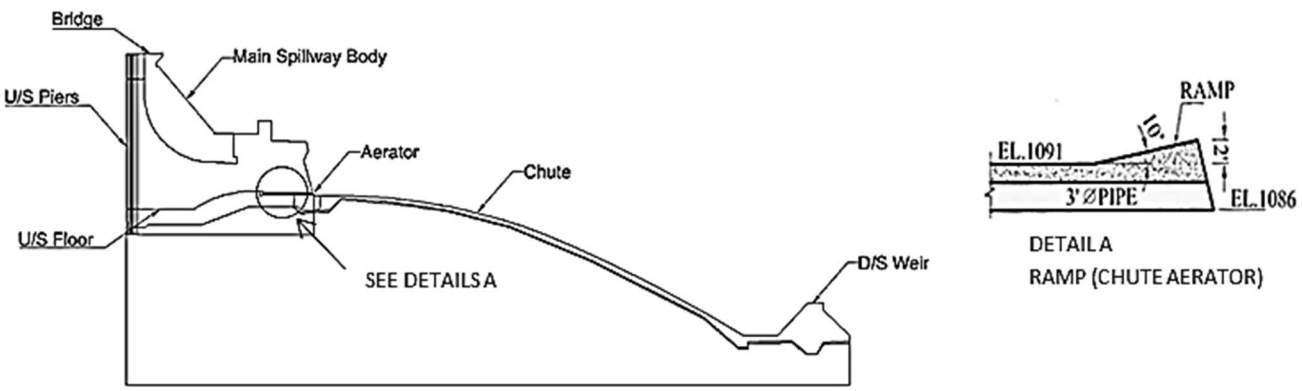

Fig. 1 Longitudinal section of Mangla Dam Spillway up to first stilling basin

2 Methodology

The following methodology was adopted for CFD modeling of Mangla Dam Spillway.

2.1 Pre-processing

In the pre-processing, a stepwise procedure was adopted.

2.1.1 Creation of Spillway Geometry

In this step, three-dimensional (3D) drawing of the spillway geometry was converted into stereolithographic (STL) format to import into CFD code FLOW 3D as an input file.

2.1.2 Mesh Generation

The accuracy of CFD solution depends on cell size. Critical mesh cell size was determined through grid convergence index (GCI). Hence, three different sets of meshes with sizes of 2.26 m, 1.5 m, and 1 m were selected to carry out grid convergence for coarse to fine size of the mesh, and the simulations were carried out to determine the discharge. During this process, the mesh size was kept uniform (single Cartesian type) throughout the entire domain. The discretization errors and GCI were calculated for all three grids as shown in Table 1. f_1, f_2, and f_3 are the solutions obtained from fine, medium, and coarse mesh, respectively, in terms of discharge, $e_{21}=\left|\frac{f_2-f_1}{f_2}\right|$ and $e_{32}=\left|\frac{f_3-f_2}{f_3}\right|$ are the approximate relative errors, and $GCI_1=\frac{1.25e_{21}}{r^p-1}$ and $GCI_2=\frac{1.25e_{32}}{r^p-1}$ are the GCIs for fine and coarse solutions, respectively, where r^p is the refinement factor with order of accuracy "p". It is seen that the GCI value in the fine-grid solution is smaller than the GCI value in the coarse-grid solution (GCI_2). Similarly, the approximate relative error is also less with a reduction in grid size.

Based on the above analysis, the grid size of 1 m was finalized for further simulations as the change in the results is less after the grid size of 1.5 m. Further decrease in grid size will increase the mesh count of the problem, and it would be difficult to simulate on the desktop computer. During mesh generation, cell aspect ratio and adjacent cells ratio were kept close to unity to ensure the quality of the mesh.

2.1.3 Boundary and Initial Condition

The fourth step in pre-processing deals with boundary and initial conditions. Boundary conditions should match with the physical conditions of the problem (Chanel and Doering 2008). Three different combinations of boundary conditions were tested during this study (Table 2). In Table 2, **Pressure** boundary condition specifies the Pressure. If fluid elevation is specified, the pressure at boundary will follow hydrostatic pressure distribution. **Out Flow** boundary condition is used to translate any flow quantity across the boundary/computational domain. **Symmetry** applies the zero-velocity conditions normal to the boundary. **Vol. Flow Rate** applies the specified flow rate at boundary whereas **Wall** relates the no-slip conditions at boundary.

Sensitivity analysis was performed to select the appropriate combination of boundary conditions. For this purpose, model was operated at a reservoir level of 378 m AMSL and 384 m AMSL with full gate opening to compare the water levels with physically observed ones for all combinations of boundary conditions. Comparison of results shown in Table 3 indicates that water levels computed with boundary condition combination 2 are closer to the physical model results. Hence, boundary conditions mentioned under combination 2 were selected for further simulation.

In Fig. 2 and Table 2, X_{min} = Upstream side of the model, X_{max} = Downstream side of the model, Y_{min} = Left side of the model Y_{max} = Right side of the model Z_{min} = Bottom side of the model, Z_{max} = top side of the model.

In all simulations conducted in this study, the rectangular fluid region as an initial condition was specified on the upstream side of the spillway at the same level as the

Table 2 Combination of boundary conditions

Boundary Extent	Combination 1	Combination 2	Combination 3
X_{min}	Pressure	Vol. flow rate	Vol. flow rate
X_{max}	Out flow	Out flow	Out flow
Y_{min}	Wall	Wall	Symmetry
Y_{max}	Wall	Wall	Symmetry
Z_{min}	Wall	Wall	Symmetry
Z_{max}	Pressure	Pressure	Pressure

Table 1 Discretization error of model for three different grid sizes

Reservoir level (m AMSL)	The mass flow rate in m^3/s			Φ_{21} (m^3/s)	Φ_{32} (m^3/s)	e_{21}	e_{32}	GCI_1 (%)	GCI_2 (%)
	$f_{1(1m)}$	$f_{2(1.5m)}$	$f_{3(2.26m)}$						
378.54	2089.4	2091.2	2094.4	1.34	3.2	6.4×10^{-4}	1.5×10^{-3}	5.6×10^{-4}	1.1×10^{-3}
384.05	2228.9	2229.6	2234.2	0.56	4.74	2.5×10^{-4}	2.1×10^{-3}	2.2×10^{-4}	1.8×10^{-3}

$\Phi_{21}=(f_2-f_1)$ and $\Phi_{32}=(f_3-f_2)$

Table 3 Percentage error in water levels with boundary conditions: (a) combination 1, (b) combination 2, (c) combination 3

Sr. No	Operating conditions		Average value of physically observed water levels (m)	Average value of numerically computed water levels (m)	Error (%)
	R/ L(m AMSL)	G/O (m)			
(a)					
1	378.54	10.67 (fully open)	325.32	328.09	0.84
2	384.05		325.72	328.51	0.85
(b)					
1	378.54	10.67 (fully open)	325.32	326.24	0.28
2	384.05		325.72	326.52	0.24
(c)					
1	378.54	10.67 (fully open)	325.32	326.95	0.50
2	384.05		325.72	327.42	0.52

R/L, reservoir level; G/O, gate opening

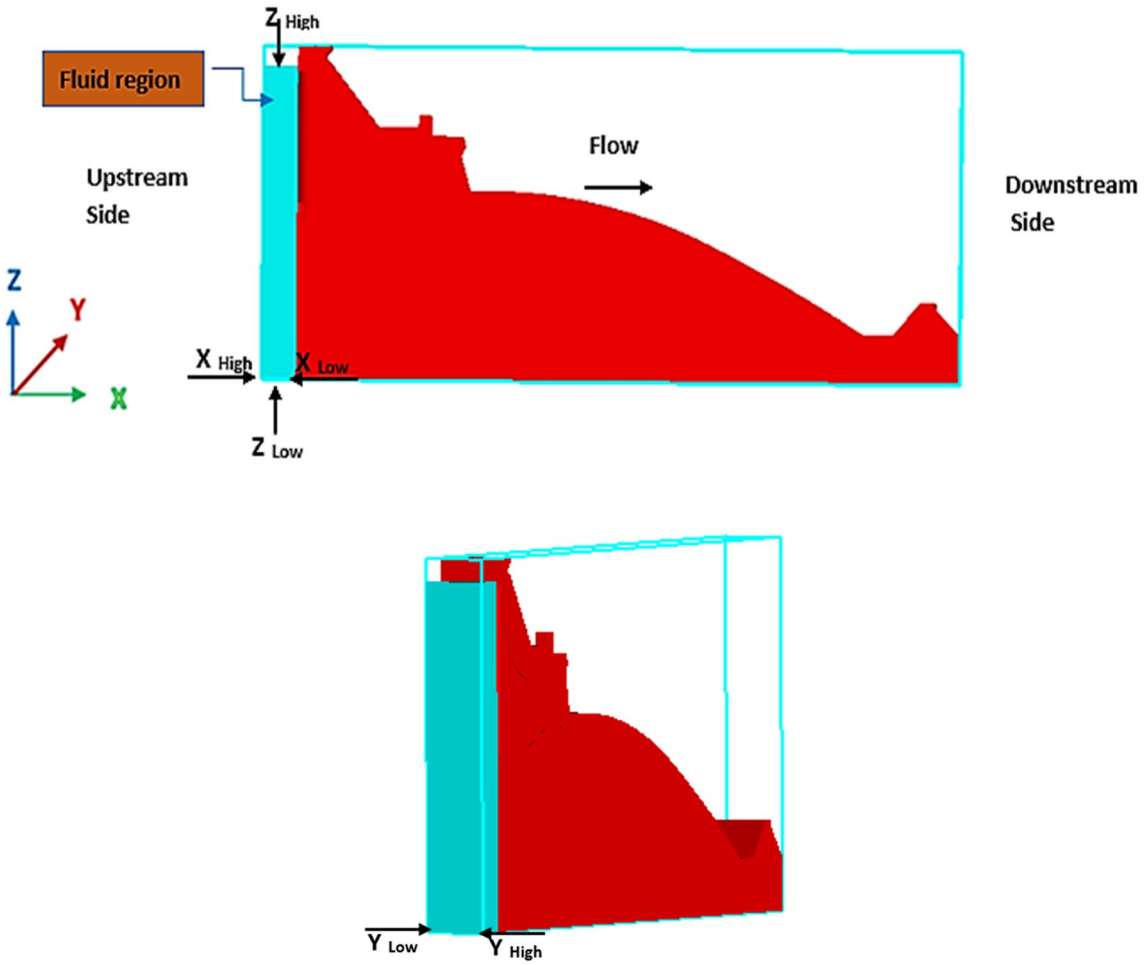

Fig. 2 The initial condition for the Mangla Spillway model

specified fluid height at the upstream boundary. This initialization is shown in Fig. 2. Small initial velocity in the x-direction was also specified to reduce simulation times. X_{High}, X_{Low}, Y_{High}, Y_{Low}, Z_{High}, and Z_{Low} were extents of the fluid region in the *x*-, *y*-, and *z*-direction. X_{High} extent of the fluid region was the upstream face of the spillway, whereas Z_{High} was the reservoir level.

2.1.4 Numerical Simulations in FLOW 3D

For the current study, numerical modeling of Mangla Dam Spillway flows and chute aerator was carried using CFD code FLOW 3D. It was selected due to its ability to model the free surface flows using the volume of fluid method (VOF). This method adopts the accurate pressure and kinetic boundary conditions. It describes the movement between two fluids in order to prevent the boundary face from smearing (Hirt and Nichols 1981). VOF method defines the cells as empty, full, and partially full with fluid. It assigns the value of zero, one (01), between zero and one (01) to empty, full, and partially full cells, respectively (Savage and Johnson 2001). The evolution of the *m*th fluid in a system on *n* fluids is governed by the transport equation as follows:

$$\frac{\partial C_m}{\partial t} + v.\nabla C_m = 0. \tag{1}$$

In Eq. (1), C_m is fraction function t is time and v is the velocity vector.

The ability to model the wall roughness, air entrainment, and cavitation was also an important consideration in selecting the FLOW 3D. To determine the void or flow region in each cell, FLOW 3D uses the fractional area/volume obstacle representation (FAVOR) method. Moreover, FLOW 3D uses multi-block mesh to model large domain and nested mesh to capture more flow details in the area of interest (Ho and Riddette 2010). FLOW 3D provides a number of methods to track fluid interfaces. There are two main types of fluid interfaces: a diffuse interface and a sharp interface. Code automatically selected the best-fit option depending on the number of fluids (Flow sciences 2013).

For practical purposes, the re-normalized group k–ε turbulent energy dissipation equation is used in spillway modeling (Ho and Riddette 2010). Governing equations for FLOW 3D are continuity and momentum equations shown as follows:

Continuity:

$$\frac{\partial}{\partial x}\left(uA_x\right) + \frac{\partial}{\partial y}\left(vA_y\right) + \frac{\partial}{\partial z}\left(wA_z\right) = 0 \tag{2}$$

Momentum:

$$\frac{\partial U_i}{\partial t} + \frac{1}{V_F}\left(U_j A_j \frac{\partial U_i}{dx_j}\right) = -\frac{1}{\rho}\frac{\partial P'}{dx_i} + g_i + f_i. \tag{3}$$

In the above equations, variables *u, v,* and *w* represent the velocities in the x-, y-, and z-directions; V_F is the volume fraction of fluid in each cell; A_x, A_y, and A_z are the fractional areas open to flow in the subscript directions; ρ is the density; P' is defined as the pressure; g_i is the gravitational force in the subscript direction; f_i represents the Reynolds stresses; and A_j is the cell face areas. Equations 2 and 3 are partial differential equations. They are discretized in both time and space. Due to the complex nature of turbulence, it is often simplified and approximated using an average approach (e.g., Reynolds-averaged Navier–Stokes).

Different options are available in the numeric tab of FLOW 3D to solve the above described governing equations of the model. In all simulations, momentum and continuity equations were solved using first-order momentum advection. FLOW 3D uses first-order upwind differencing method for momentum advection algorithm (a transport mechanism of a momentum or conserved property by a fluid due to the fluid's bulk motion). It is robust and sufficiently accurate method in most situations (Flow Sciences 2013). Default time step control was used unless simulation would crash. In that case, a smaller minimum time step was tried to obtain the converging solution. All simulations were completed by using the explicit solver option. In this option, the solution is solved progressively at each computational cell by stepping through time, while the time step is restricted to meet stability criteria. The model also provides two pressure solver options namely successive over-relaxation (SOR) and the generalized minimum residual (GMRES). Both options provide fairly good and similar results. In this study, the SOR pressure solver option was used as it ran the simulation slightly faster than GMRES. The iterative convergence is achieved with at least three orders of magnitude decrease in the normalized residuals for each equation solved. Iterative convergence at each time step was checked. Each time step had 30 iterations, and all residuals dropped under three orders every time step. Iterative convergence was achieved in about 600 steps (18,000 iterations) for achieving steady-state discharge.

2.2 Validation of Model

Validation of the numerical model is very important to check its accuracy. True validation of numerical model includes the comparison of model result with prototype measurements. But Mangla Dam Spillway model was validated using physical model results due to lack of prototype data. The physical model of the Mangla Dam Spillway was constructed by Water and Power Development Authority (WAPDA) on an undistorted scale of 1:36 (Wapda 2004) as shown in Fig. 3.

During physical modeling, some dimensionless numbers were also studied. In this case, Re (Reynolds number) = 2.67×10^6, We (Weber number) = 509, and Froude number (Fr. No.) varied between 2 and 7. Model discharge was measured with suppressed sharp-crested weir. It was installed downstream of the model to measure the flow at different reservoir levels and gate opening. Staff gauge graduated to model scale was used to record the water levels. Total 15 points were marked along the centerline of the chute to observe the water levels, whereas velocity and

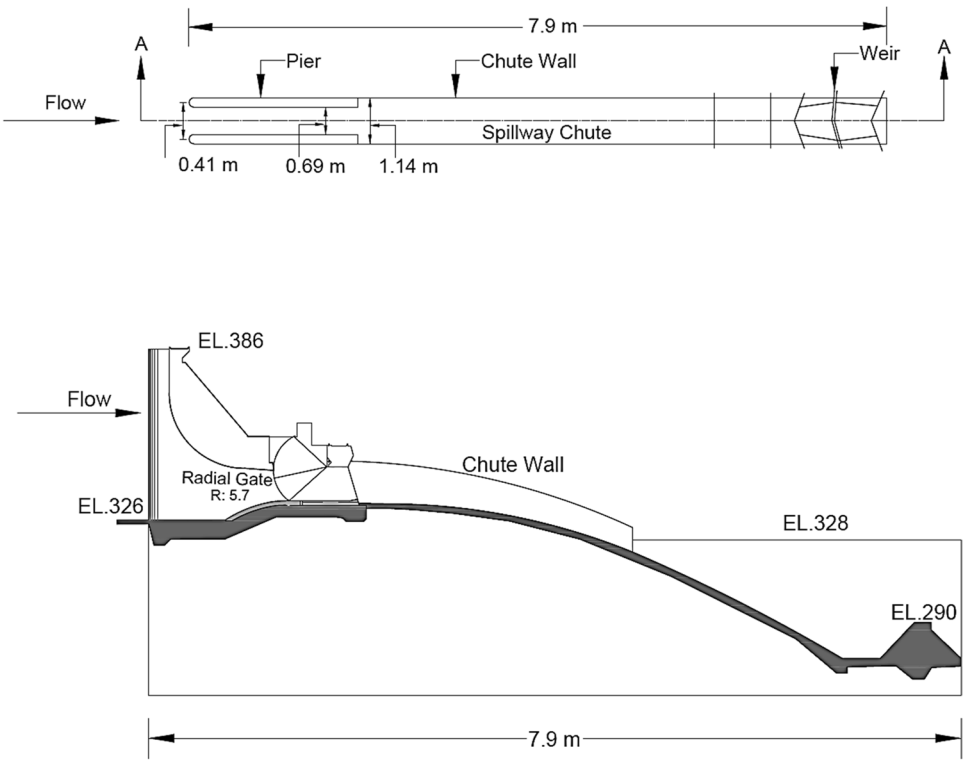

Fig. 3 Plan and longitudinal section of physical model of Mangla Dam Spillway at 1:36 scale

pressure were also measured at the same 15 observation points with current meter and transducer, respectively. These observation points were also located on the CFD model by using their co-ordinates. But for validation purposes, only a single point near the start of the chute was selected to get computed values of flow parameters and Froude number, while discharge value was computed at outflow boundary condition ($X_{max.}$) by using the "mesh dependent history output" option of the CFD model.

Comparison of computed parameters and observed one is shown in Table 4a, b. Table 4a shows that numerical model results match well with physical model data for selected operating conditions. Similarly, in Table 4b, a comparison of results indicates the numerical model data are in good agreement with physical model data. In both cases, the relative error is within 6%, which indicates that the numerical model can be confidently used for further simulations (Chanel and Doering 2008).

2.3 Model Operation

After validation, the model was operated between conservation level and highest flood level with two different gate openings to assess the hydraulic performance of the spillway. Flow parameters including discharge, velocity, chute bottom pressures, and water surface profiles were computed by using the operating conditions shown in Table 5. But, to assess the performance of the chute aerator, the volume fraction of

Table 4 (a, b) Validation of Mangla Spillway CFD model

Sr. no.	Flow characteristic	Scale model results	CFD model results
(a)			
Operating condition 1: Reservoir Level = 378.54 m AMSL, Gate Opening = 10.67 m			
1	Discharge(m^3/s)	2078.20	2089.86
2	Flow velocity (m/s)	26.21	26.64
3	Water level at the crest	343.20	343.44
4	Chute pressure head (m) at just ahead of chute aerator	5.99	5.67
5	Froude number	2.85	2.68
(b)			
Operating condition 2: Reservoir Level = 384.05 m AMSL, Gate Opening = 10.67 m			
1	Discharge(m^3/s)	2222.76	2225.92
2	Flow velocity (m/s)	27.28	29.32
3	Water level at crest	343.29	343.80
4	Chute pressure head (m) at just ahead of chute aerator	5.68	5.42
5	Froude number	2.90	2.76

Table 5 Model operating condition

Reservoir levels	Gate opening
380 m AMSL	6.10 m
	9.14 m
381 m AMSL	6.10 m
	9.14 m
383 m AMSL	6.10 m
	9.14 m

entrained air was computed by operating the model at full gate opening (10.6 m) against 378 m AMSL (conservation level) and 384 m AMSL (highest flood level). The volume fraction of entrained air was computed at two locations of spillway chute, i.e., L_1 and L_2, where L_1 = location just after the reattachment of the jet length and L_2 = location before the entry point of the energy dissipation system.

2.4 Post-processing

In post-processing, flow parameters were computed by using the model operating conditions shown in Table 3. Plots were drawn for water levels, velocities, and pressure distribution along the spillway chute to evaluate the hydraulic performance of Mangla Spillway, while profiles for the volume fraction of entrained air were drawn with ramp of different heights (0.4 m, 0.5 m and 0.6 m) and without ramp to assess the performance of the aerator.

3 Results and Discussion

3.1 Computation of Pressures along Spillway Chute

Pressures are computed along the spillway chute to avoid cavitation damages as it causes the fatigue failure of chute concrete. Figure 4 indicates pressure variation along the spillway chute at three reservoir levels and two different gate openings (G/O). Almost similar variation is noted in all three cases. Initially, at a large gate opening, pressure values are comparatively high than a small gate opening. It is because of high flow depths. Generally, an increasing trend in pressure values is observed up to the end of the spillway chute. However, no negative pressure value is noted throughout the spillway chute.

3.2 Flow Velocity Profiles

Flow velocities are computed to evaluate the erosion potential downstream of the spillway. Hence, flow velocity profiles help in designing the energy dissipation system accordingly. Figure 5 describes the velocity profiles. Flow velocities are gradually increasing at all operating conditions. Velocity varies between 10 and 30 m/s along the chute. But it decreases near the end of spillway chute due to collision of flowing water with small height weir. Provision of double stilling basin downstream of weir further reduces the velocities, which ultimately helps in decreasing the downstream riverbed erosion.

3.3 Water Level Profile

Computation regarding water levels on spillway chute is important as it helps the designers in evaluating the risk of crossing the flood water over crest bridge and chute walls. Flood water consistently crossing over the chute walls may cause the progressive erosion of the chute foundation, which may lead to its collapse. Computed water levels are shown in Fig. 6. Negligible fluctuation in water levels is noted at all operating conditions. However, water levels are slightly varying between 150 and 230 m from the spillway axis. The highest water level computed among all three cases is 343 m AMSL which is below the top level of the chute wall. In this case, flood water will not overtop the chute wall.

3.4 Performance Evaluation of Chute Aerator

The presence of entrained air fraction in the water near the spillway chute floor is indispensable. It should be up to 6% to avoid cavitational damages. In this study, it is computed not only at spillway chute floor but also across flow depth at two locations (L_1 and L_2). The computed volume fraction of entrained air across the flow depth ratio (d/d_o) is shown in Fig. 7, whereas model output in the form of contours is given in Fig. 8. Different colors of contours show the variation of entrained air along the chute and across the flow depth. In Fig. 8b, near the end of chute, colors of the contours are different from Fig. 8a due to an increase in volume fraction of entrained air. It reflects very positive impact of the ramp installed at chute aerator. Figure 7a indicates that the volume fraction of entrained air in water, at location L_1, close to the chute floor is 3% which rises to 20% near the water surface, while the volume of entrained air in water has increased near the end of the spillway chute (at L_2) due to turbulence of flowing water and redistribution of entrained air across the flow depth.

Figure 7b–d presents the profiles for fraction of entrained air in water after the installation of the ramp of different heights (0.4 m, 0.5 m, and 0.6 m) on the chute aerator. Figure 7b–d shows that fraction of air is increasing with the increase in ramp height. The addition of ramps of different heights increased the jet length, which in turn increases the air entrainment. At location L_1, the fraction of air is varying from 6 to 28% (from bottom to top) across flow depth for all ramp heights. Water entrained more air in this case as compared without ramp on the aerator. Effect of the ramp has also

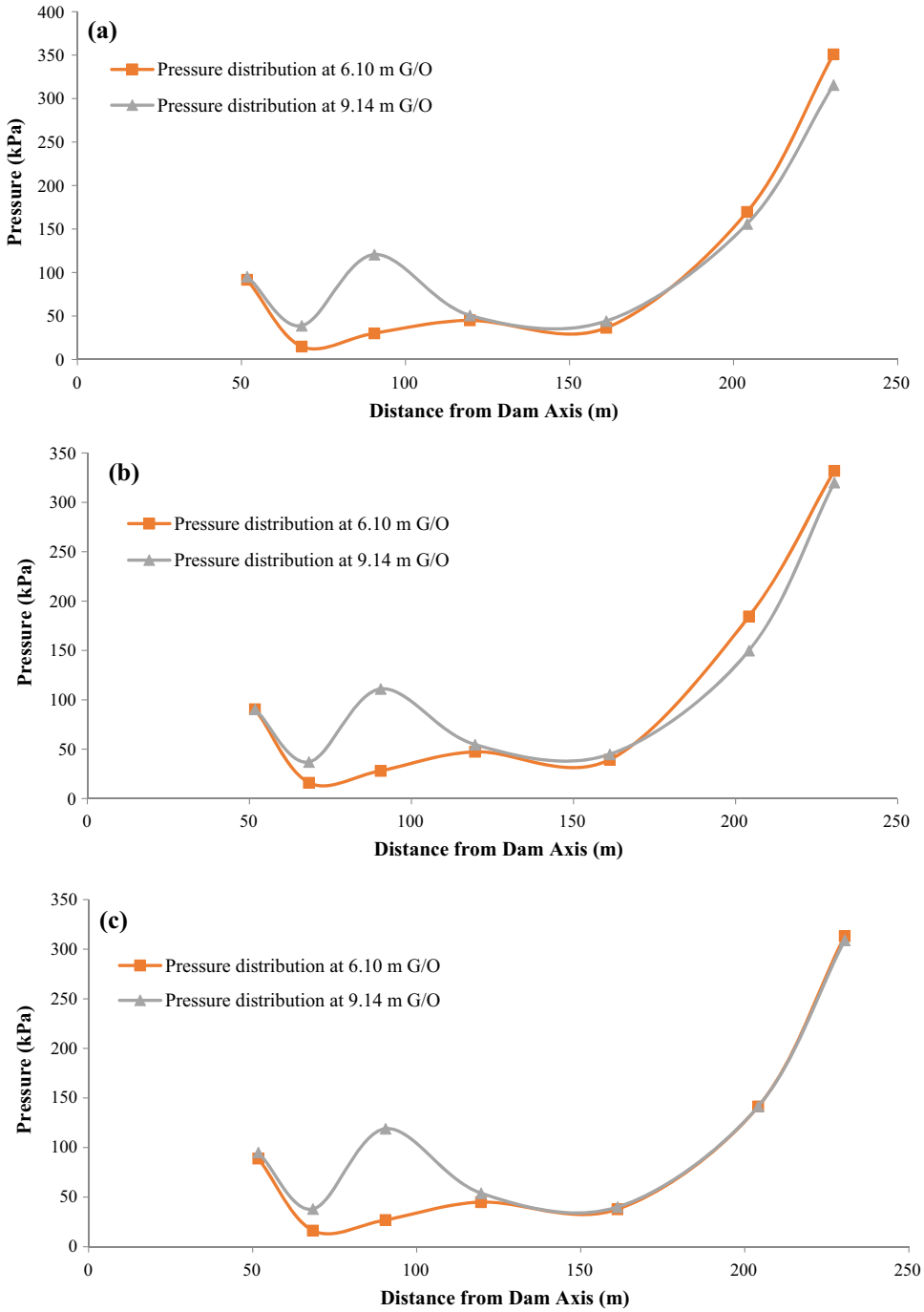

Fig. 4 Computed pressures at reservoir level: **a** 380 m AMSL, **b** 381 m AMSL, **c** 383 m AMSL

transferred to location L_2. At this location, near the bed, fraction of air fluctuates from 20 to 57%. These values indicate that the performance of the aerator has improved after the installation of ramp.

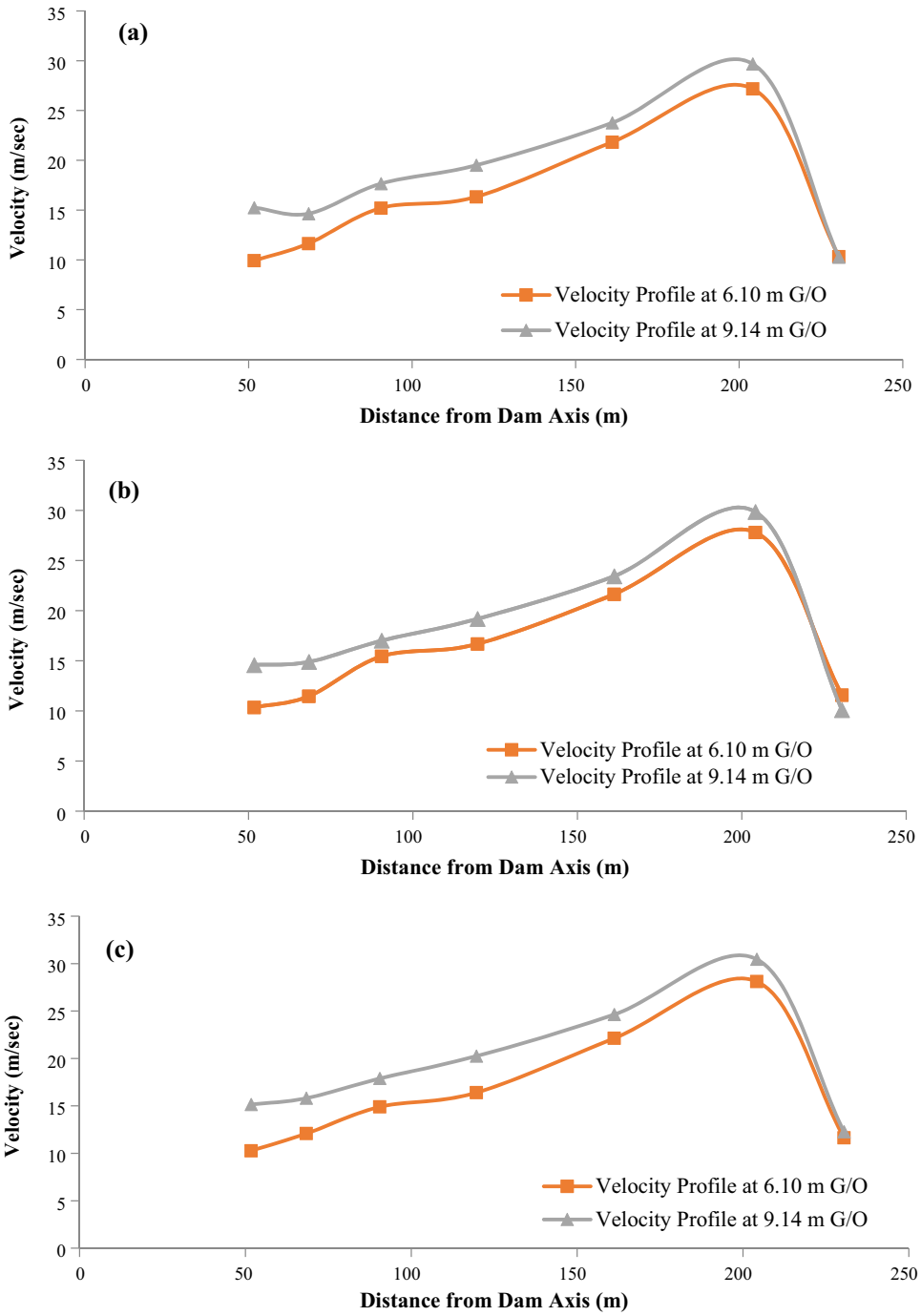

Fig. 5 Velocity profiles at reservoir level: **a** 380 m AMSL, **b** 381 m AMSL, **c** 383 m AMSL

4 Conclusions

The relative error between computed and observed flow parameters was within 6%. It confirmed that the CFD model of the Mangla Spillway can assess the hydraulic performance of the spillway and chute aerator. Pressure distribution on spillway chute varied from 10 to 350 kPa (kilopascal) in all cases. There was no risk of cavitational damage as pressure remained positive throughout the spillway chute. Velocity was found in the range of 10–30 m/s. It is reduced to 10 m/s near the entry point of the energy dissipation system. The highest water level computed by the model was 343 m AMSL, whereas the top level of the chute wall is 350 m AMSL, which indicates that flow

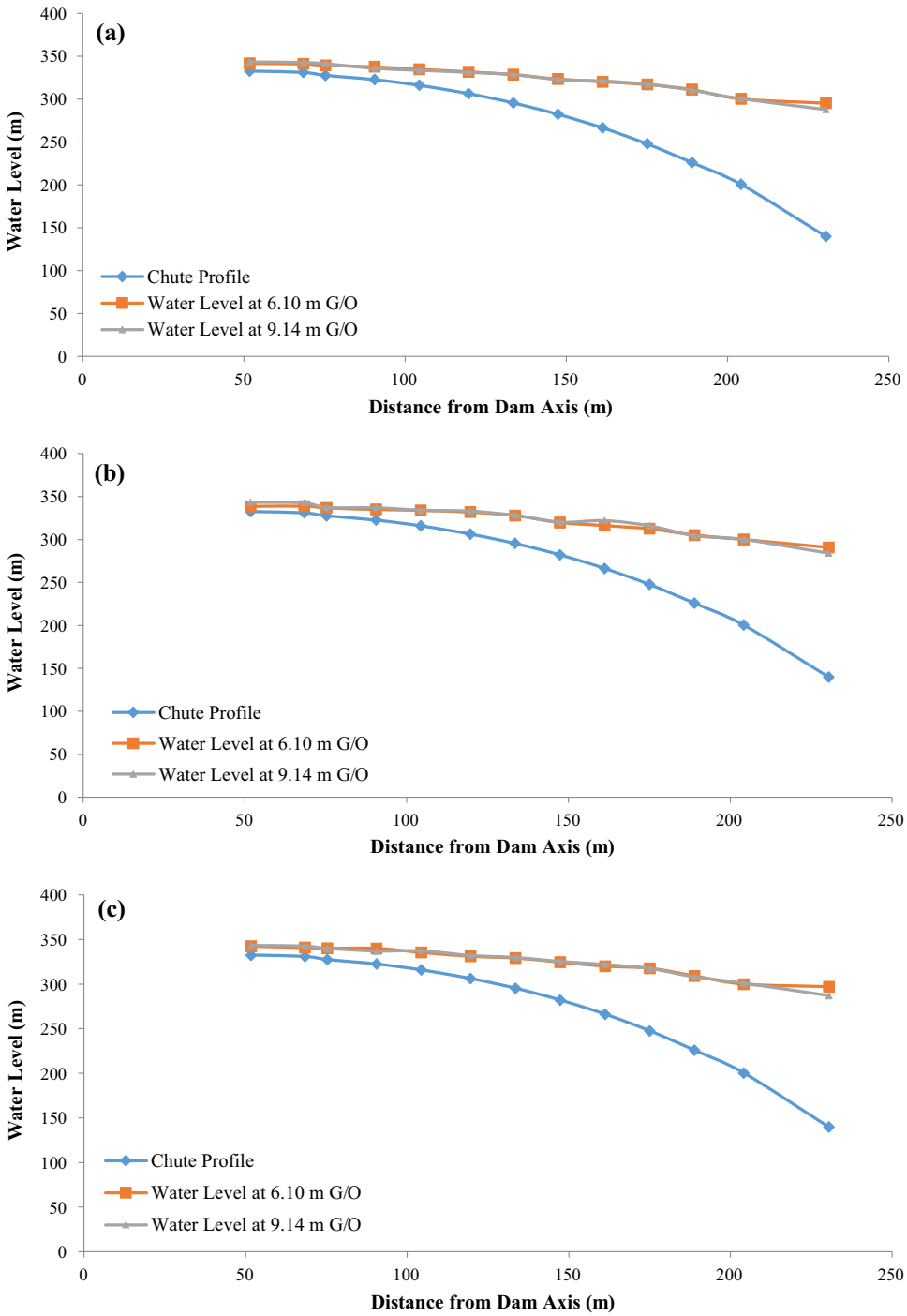

Fig. 6 Water level profile at reservoir level: **a** 380 m AMSL, **b** 381 m AMSL, **c** 383 m AMSL

will not cross the sidewalls of the spillway chute during flood operation. Performance of chute aerator was assessed by operating the model at conservation level (378.54 m AMSL) and highest flood level (384.05 m AMSL) with full gate opening. Without ramp on the aerator, air fraction near bed was 3% and 20% at location L_1 and L_2, respectively. After installation of ramp, these values raised to 6% and 57%, which was the indication of improved performance of chute aerator.

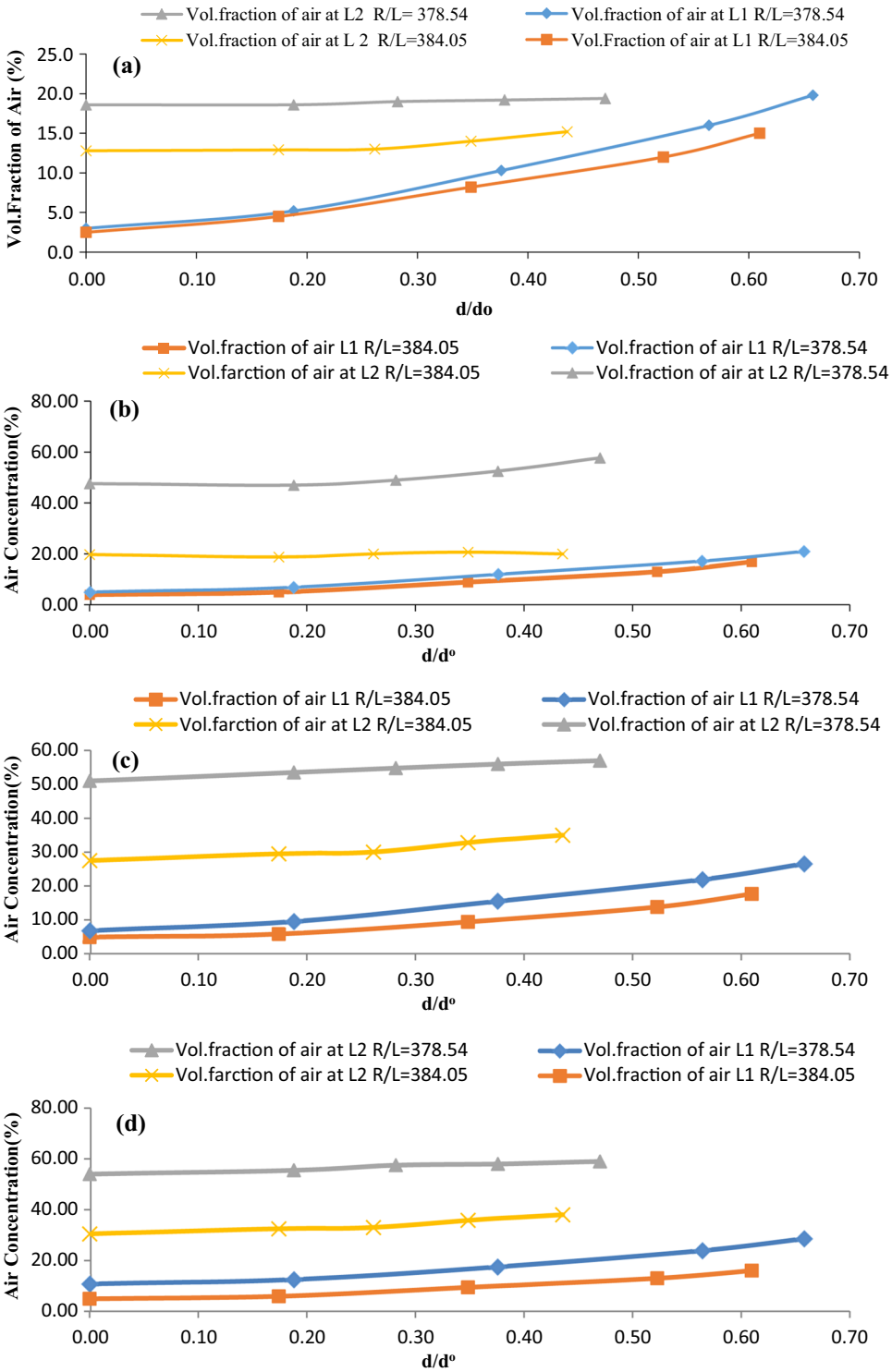

Fig. 7 The volume fraction of entrained air in water: **a** without a ramp, **b** with 0.4-m-high ramp, **c** with 0.5-m-high ramp, **d** with 0.6-m-high ramp

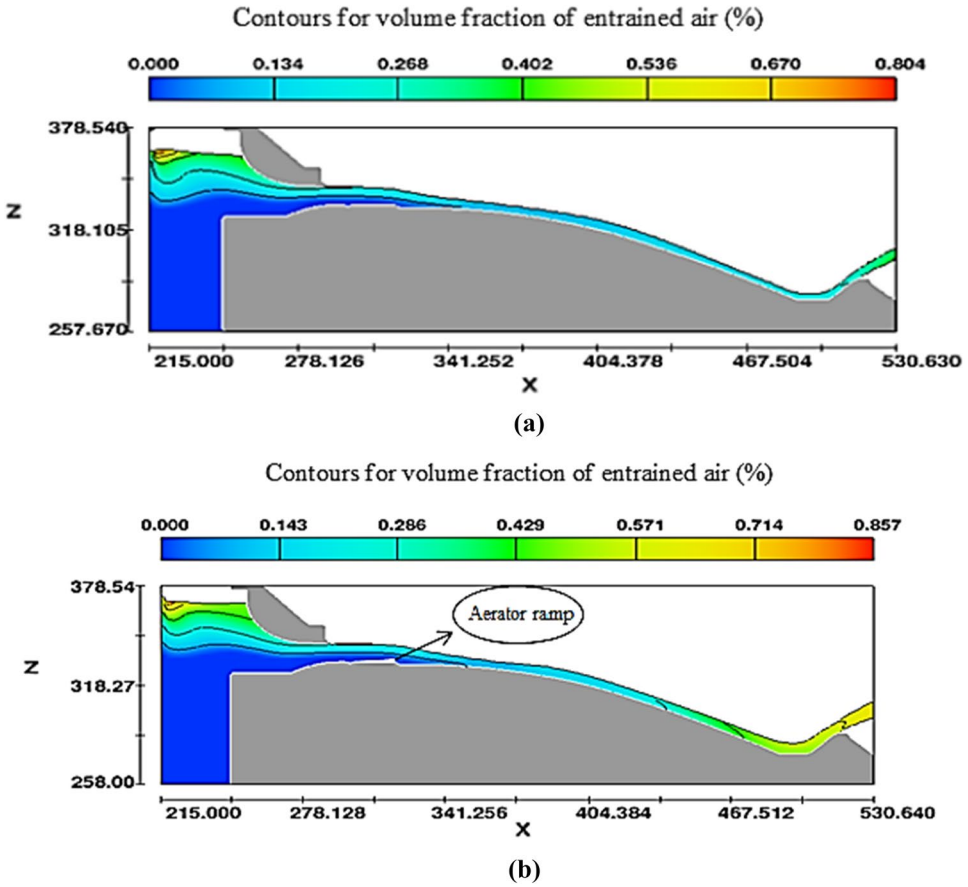

Fig. 8 Entrained air contours at reservoir level = 378.54 m AMSL: **a** without a ramp, **b** with 0.6-m-high ramp

Acknowledgements We would like to thank the Water and Power Development Authority of Pakistan for their support in providing the essential data to conduct this study.

Funding No funding was received to assist with the preparation of this manuscript.

Data Availability The data used to support the findings of this study are available from the corresponding author upon reasonable request.

Declarations

Conflict of interest The authors declare that they have no conflicts of interest to this work.

Ethics Approval Not applicable.

Consent to Participate Not applicable.

Consent to Publish Not applicable.

References

Aydin MC (2018) Aeration efficiency of bottom-inlet aerators for spillways. ISH J Hydraul Eng 24(3):330–336. https://doi.org/10.1080/09715010.2017.1381576

Bennett P, Chesterton J, Neeve D, Ucuncu M, Wearing M, Jones SEL (2018) Use of CFD for modelling spillway performance. Dams Reserv 28(2):62–72. https://doi.org/10.1680/jdare.18.00001

Bhosekar VV, Jothiprakash V, Deolalikar PB (2012) Orifice Spillway Aerator: Hydraulic Design. J Hydraul Eng 138(6):563–572. https://doi.org/10.1061/(ASCE)HY.1943-7900.0000548

Chanel PG, Doering JC (2008) Assessment of spillway modeling using computational fluid dynamics. Can J Civ Eng 35(12):1481–1485. https://doi.org/10.1139/L08-094

Flow Sciences, Inc. (2013) FLOW 3D user manual version 10.1.

Gadge PP, Jothiprakash V, Bhosekar VV (2018) Hydraulic investigation and design of roof profile of an orifice spillway using experimental and numerical models. J Appl Water Eng Res 6(2):85–94. https://doi.org/10.1080/23249676.2016.1214627

Gadge PP, Jothiprakash V, Bhosekar VV (2019) Hydraulic design considerations for orifice spillways. ISH J Hydraul Eng 25(1):12–18. https://doi.org/10.1080/09715010.2018.1423579

Gu S, Ren L, Wang X, Xie H, Huang Y, Wei J, Shao S (2017) SPHysics simulation of experimental spillway hydraulics. Water 9(12):973. https://doi.org/10.3390/w9120973

Gurav NV (2015) Physical and Numerical Modeling of an Orifice Spillway. Int J Mech Prod Eng 3(10):71–75

Hirt CW, Nichols BD (1981) Volume of fluid (VOF) method for the dynamics of free boundaries. J Comput Phys 39(1):201–225. https://doi.org/10.1016/0021-9991(81)90145-5

Ho DKH, Riddette KM (2010) Application of computational fluid dynamics to evaluate hydraulic performance of spillways in Australia. Aust J Civ Eng 6(1):81–104. https://doi.org/10.1080/14488353.2010.11463946

Jothiprakash V, Bhosekar VV, Deolalikar PB (2015) Flow characteristics of orifice spillway aerator: numerical model studies. ISH J Hydraul Eng 21(2):216–230. https://doi.org/10.1080/09715010.2015.1007093

Kumcu SY (2017) Investigation of flow over spillway modeling and comparison between experimental data and CFD analysis. KSCE J Civ Eng 21(3):994–1003. https://doi.org/10.1007/s12205-016-1257-z

Lian J, Qi C, Liu F, Gou W, Pan S, Ouyang Q (2017) Air entrainment and air demand in the spillway tunnel at the Jinping-I Dam. Appl Sci 7(9):930. https://doi.org/10.3390/app7090930

Luo M, Khayyer A, Lin P (2021) Particle methods in ocean and coastal engineering. Appl Ocean Res 114:102734

Moreira A, Leroy A, Violeau D, Taveira-Pinto F (2019) Dam spillways and the SPH method: two case studies in Portugal. J Appl Water Eng Res 7(3):228–245. https://doi.org/10.1080/23249676.2019.1611496

Moreira AB, Leroy A, Violeau D, Taveira-Pinto FA (2020) Overview of large-scale smoothed particle hydrodynamics modeling of dam hydraulics. J Hydraul Eng 146(2):03119001. https://doi.org/10.1061/(ASCE)HY.1943-7900.0001658

O'Connor J, Rogers BD (2021) A fluid–structure interaction model for free-surface flows and flexible structures using smoothed particle hydrodynamics on a GPU. J Fluids Struct. https://doi.org/10.1016/j.jfluidstructs.2021.103312

Sarwar MK, Bhatti MT, Khan NM (2016) Evaluation of air vents and ramp angles on the performance of orifice spillway aerators. J Eng Appl Sci 35(1):85–93

Sarwar MK, Ahmad I, Chaudary ZA, Mughal H-U-R (2020) Experimental and numerical studies on orifice spillway aerator of Bunji Dam. J Chin Inst Eng 43(1):27–36. https://doi.org/10.1080/02533839.2019.1676652

Saunders K, Prakash M, Cleary PW, Cordell M (2014) Application of smoothed particle hydrodynamics for modelling gated spillway flows. Appl Math Model 38(17–18):4308–4322. https://doi.org/10.1016/j.apm.2014.05.008

Savage BM, Johnson MC (2001) Flow over ogee spillway: physical and numerical model case study. J Hydraul Eng 127(8):640–649. https://doi.org/10.1061/(ASCE)0733-9429(2001)127:8(640)

Shadloo MS, Oger G, le Touzé D (2016) Smoothed particle hydrodynamics method for fluid flows, towards industrial applications: Motivations, current state, and challenges. Comput Fluids. https://doi.org/10.1016/j.compfluid.2016.05.029

Shao Z, Jahangir Z, MuhammadYasir Q, Atta-ur-Rahman, Mahmood S (2020) Identification of potential sites for a multi-purpose dam using a dam suitability stream model. Water 12(11):3249. https://doi.org/10.3390/w12113249

Shimizu Y, Khayyer A, Gotoh H, Nagashima K (2020) An enhanced multiphase ISPH-based method for accurate modeling of oil spill. Coast Eng J 62(4):625–646. https://doi.org/10.1080/21664250.2020.1815362

Teng P, Yang J (2016) CFD modeling of two-phase flow of a spillway chute aerator of large width. J Appl Water Eng Res 4(2):163–177. https://doi.org/10.1080/23249676.2015.1124030

Teng P, Yang J, Pfister M (2016) Studies of two-phase flow at a chute aerator with experiments and CFD modelling. Model Simul Eng 2016:1–11. https://doi.org/10.1155/2016/4729128

Wapda (2004) Mangla dam raising project-sectional physical model study report of main spillway: Wapda model study cell, Gujrawala, Pakistan

Yang J, Andreasson P, Teng P, Xie Q (2019) The past and present of discharge capacity modeling for spillways—a Swedish perspective. Fluids 4(1):10. https://doi.org/10.3390/fluids4010010

Yang J, Teng P, Xie Q, Li S (2020) Understanding water flows and air venting features of spillway—a case study. Water 12(8):2106. https://doi.org/10.3390/w12082106

Ye T, Pan D, Huang C, Liu M (2019) Smoothed particle hydrodynamics (SPH) for complex fluid flows: recent developments in methodology and applications. Phys Fluids 31(1):011301

Zhan X, Qin H, Liu Y, Yao L, Xie W, Liu G, Zhou J (2020) Variational Bayesian neural network for ensemble flood forecasting. Water 12(10):2740. https://doi.org/10.3390/w12102740